ARTICLES

Miscible quarter five-spot displacements in a Hele-Shaw cell and the role of flow-induced dispersion

Philippe Petitjeans
Laboratoire de Physique et Mécanique des Milieux Hétérogènes (LPMMH), Ecole Supérieure de Physique et de Chimie Industrielles (ESPCI), 10, rue Vauquelin—75231 Paris, Cedex 05, France and Department of Aerospace and Mechanical Engineering, University of Southern California, Los Angeles, California 90089-1191

Ching-Yao Chen
Department of Aerospace and Mechanical Engineering, University of Southern California, Los Angeles, California 90089-1191

Eckart Meiburg[a] and Tony Maxworthy
Laboratoire de Physique et Mécanique des Milieux Hétérogènes (LPMMH), Ecole Supérieure de Physique et de Chimie Industrielles (ESPCI), 10, rue Vauquelin—75231 Paris, Cedex 05, France and Department of Aerospace and Mechanical Engineering, University of Southern California, Los Angeles, California 90089-1191

(Received 7 October 1998; accepted 30 March 1999)

Miscible quarter five-spot displacements in a Hele-Shaw cell are investigated by means of experimental measurements and numerical simulations. The experiments record both the volumetric as well as the surface efficiency at breakthrough as a function of the dimensionless flow rate in the form of a Peclet number and the viscosity contrast. For small flow rates, both of these efficiency measures decrease uniformly with increasing Peclet numbers. At large flow rates, an asymptotic state is reached where the efficiencies no longer depend on the Peclet number. Up to Atwood numbers of approximately 0.5, the less viscous fluid occupies close to $\frac{2}{3}$ of the gap width, which indicates a near-parabolic velocity profile across the gap. Consequently, in this parameter range a Taylor dispersion approach should be well suited to account for flow-induced dispersion effects. For larger viscosity contrasts, accompanying two-dimensional numerical simulations based on Taylor dispersion predict an increased stabilization for high flow rates, which is not confirmed by the experiments. This suggests that, in order to extend the range of applicability to larger viscosity contrasts, the components of the dispersion tensor will have to be amended in order to account for the presence of quasi-steady fingers. © *1999 American Institute of Physics.* [S1070-6631(99)01707-9]

I. INTRODUCTION

Hele-Shaw flows have long served as models for exploring the dynamics of both miscible and immiscible porous media displacements.[1,2] While most investigations have addressed unidirectional flows, the quarter five-spot arrangement of injection and production wells represents the preferred configuration for evaluating the important role of localized sources and sinks on the flow. Already the early porous media experiments by Caudle and Witte,[3] Simmons *et al.*,[4] Habermann,[5] and Lacey *et al.*[6] show how, for unfavorable mobility ratios, the growth of viscous fingers adversely affects the sweep efficiency. The authors provide data for this efficiency measure at the time of breakthrough and beyond, as a function of the viscosity contrast between the fluids. Hele-Shaw experiments for the quarter five-spot geometry were conducted by Mahaffey *et al.*[7] as well as Todd and Longstaff.[8] A more recent investigation by Zhang *et al.*[9] presents both experimental and numerical results for quarter five-spot displacements in porous media, with good agreement between the two regarding the overall efficiency of the process. For a more complete recent review of related work, cf. Refs. 10 and 11.

For miscible displacements in porous environments, it is well known that the large-scale features of the evolving concentration field are determined not only by the properties of the fluids, such as their densities and viscosities, but also by the way in which the structure of the porous medium itself affects the small scales of the velocity field. In a classical

[a]Author to whom correspondence should be addressed. Electronic mail: eckart@spock.usc.edu

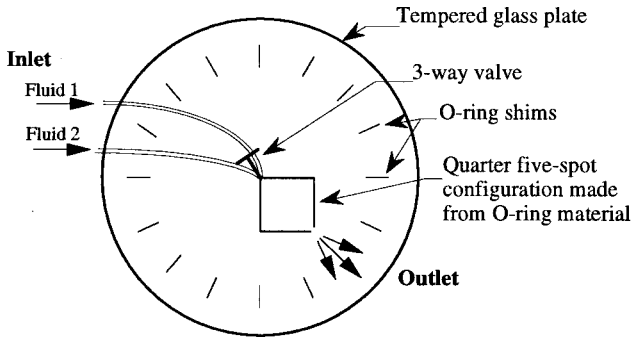

FIG. 1. Experimental set-up.

paper, Taylor[12] investigated this flow-induced dispersion for the case of a passive tracer added to a Poiseuille flow in a tube. He showed that, even in the absence of molecular diffusion in the streamwise direction, the flow resulted in an error function profile of the concentration averaged over the tube's cross section. Thus, the convective motion of the fluid is seen to affect the large-scale features of the averaged concentration profile in a fashion that is somewhat similar to a diffusion process. This result was employed by Mahaffey *et al.*[7] in order to compare the effects of diffusion in their Hele-Shaw experiments to those in a large-scale field application. Horne and Rodriguez[13] applied Taylor's approach to Poiseuille flow in a plane channel and arrived at a similar result for this geometry. An overview of the relevant mechanisms resulting in dispersion is given by Brady and Koch.[14] In a typical miscible porous media displacement, this flow-induced dispersion process plays a dominant role in establishing the concentration front thickness, and thereby determines the length scales of potential instabilities that can evolve as a result of unfavorable viscosity or density gradients. It is hence crucial that theoretical and numerical analyses of such displacements account for this effect. In large-scale simulations, this usually cannot be accomplished in a straightforward way, i.e., by resolving the flow at all length scales, since the large scales of the displacement are too disparate from the pore scale. Consequently, the effects of flow-induced dispersion on the overall flow need to be modeled. Based on the early work by Peaceman and Rachford,[15] the numerical simulations of Ewing *et al.*[16] hence employ a velocity-dependent dispersion tensor, with empirically determined values for the longitudinal and transverse dispersion coefficients. Yortsos and Zeybek,[17] in their investigation of the effects of dispersion on the stability of rectilinear displacements, use a simple model first suggested by Bear.[18] Surprisingly, they find dispersion to be destabilizing at short wavelengths. Zimmerman and Homsy[19] present two-dimensional, fully nonlinear spectral simulations of rectilinear miscible porous media displacements involving a velocity-dependent dispersion tensor whose components do not involve any empirical constants. Instead, the authors make use of the results by Horne and Rodriguez[13] in order to establish the required relationships between the tensor components and the local velocity field. While suggesting that this approach is appropriate for both porous media and Hele-Shaw flows, the authors do point out that assuming the existence of a Poiseuille flow profile for variable viscosity fluids represents a simplifying assumption. At high Peclet numbers and for long times, their simulations show the interesting result that some of the large-scale flow features become independent of the Peclet number, which suggests that the details of the concentration field are of limited importance. A similar approach is taken in the numerical simulations of Zhang *et al.*[9]

The recent experimental observations by Petitjeans and Maxworthy,[20] as well as the accompanying numerical simulations of Chen and Meiburg[21] raise some questions regarding the range of viscosity contrasts for which the Taylor dispersion model is applicable to Hele-Shaw flows for large Peclet numbers, cf. also the results by Yang and Yortsos[22] and Rakotomalala *et al.*[23] For large dimensionless flow rates and strong viscosity contrasts, the Stokes flow simulation results of Chen and Meiburg[21] show that miscible displacements in a two-dimensional gap result in the development of a quasi-steady state, which is characterized by a finger of the less viscous fluid propagating along the centerline of the gap. In a reference frame moving with the tip of this finger, the concentration field in the vicinity of the front then remains nearly constant. For this flow, the velocity profile across the gap is quite different from the parabolic shape assumed by Taylor and Horne and Rodriguez. The temporal and spatial evolution of the concentration profile averaged over the tube's cross section thus proceeds in a distinctly different fashion from the spreading error function found by these authors. For smaller viscosity contrasts and at lower values of the Peclet number, on the other hand, such a quasi-steady state never develops, and the velocity profile is approximately of Poiseuille shape. Hence it will be of interest to reassess, through a combined experimental and computational effort, the parameter range in which the Taylor dispersion model is applicable to miscible displacements in a Hele-Shaw cell. This will be a primary goal of the present investigation.

A final point of interest for miscible displacements concerns the potential importance of additional stresses near the concentration front that are not accounted for by the Navier-Stokes equations. Such stresses were first postulated by Korteweg,[24] but subsequently were given little attention. More recently, the investigations by Davis,[25] as well as by Joseph and collaborators (Joseph,[26] Joseph and Hu,[27] Joseph and Renardy[28]), have placed a renewed emphasis on this topic, as they raise the possibility of an effective surface tension in miscible fluids, cf. also Petitjeans[29] and Petitjeans and Kurowski.[30] In the context of comparisons between experimental and numerical observations, this topic is discussed by Chen and Meiburg[21] as well as by Petitjeans and Maxworthy.[20]

The outline of the paper is as follows. In Sec. II we will describe the Hele-Shaw cell and the miscible displacement experiments conducted in it. The experiments will be analyzed both by means of flow visualization as well as by several quantitative measures related to the sweep efficiency. In Sec. III we will present numerical simulation results for miscible quarter five-spot flows in a Hele-Shaw configuration, obtained with a Taylor dispersion model based on

TABLE I. Parameters of experimental runs.

Fluid 1 (more viscous)	Fluid 2 (less viscous)	At	M
Mixture, $c_g=42.7\%$	water + dye	0.537	3.32
Mixture, $c_g=49.3\%$	water + dye	0.635	4.48
Mixture, $c_g=66.4\%$	water + dye	0.848	12.2
Mixture, $c_g=96.0\%$	Mixture, $c_g=76.9\%$	0.848	12.2
Mixture, $c_g=82.9\%$	water + dye	0.982	110
Mixture, $c_g=90.5\%$	water + dye	0.987	153

Horne and Rodriguez's[13] results, cf. Ref. 19. Some interesting features of this model will be pointed out, and their effect on the simulation results will be discussed. Finally, in Sec. IV we will discuss the experimental and numerical observations, in order to obtain information regarding the validity of the Taylor dispersion model for Hele-Shaw displacements.

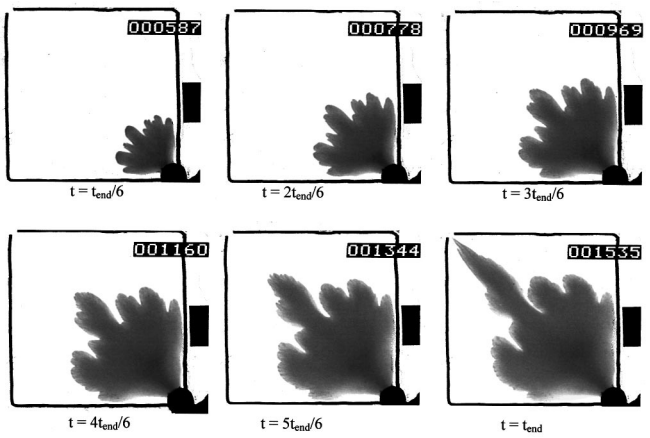

FIG. 2. Example of the development of the instability at six different times, up to the time t_{end} of breakthrough. Here, a water-dye mixture displaces a glycerin-water mixture of concentration $c_g=66.4\%$. The Atwood number is 0.848, and the Peclet number has a value of approximately 13 500. The numbers in the upper right corners of the picture indicate the video frame.

II. EXPERIMENTS

A. Setup

The experiments are conducted in a horizontally arranged, circular Hele-Shaw cell formed by two 1.9 cm thick, tempered glass plates of 68 cm diameter (Fig. 1). Under the moderate pressures applied in the current experiments, these plates do not exhibit any significant bending, and a constant gap width $d=0.61$ mm is maintained with high accuracy. An O-ring is employed to seal the gap and establish a quarter five-spot configuration of side length $L=100$ mm within the central portion of the cell. Additional short O-ring segments are uniformly distributed along the circumference of the cell in order to further minimize bending of the plates. The fluid enters the cell through a 0.4 mm diameter hole at the center of one of the plates (in one corner of the quarter five-spot geometry), and exits along its entire circumference. The exit from the quarter five-spot arrangement consists of a 4 mm wide gap in the O-ring.

The Hele-Shaw cell is initially occupied by the more viscous fluid, in this case a glycerin-water mixture. The less viscous fluid, a water-dye or glycerin-water-dye mixture with a smaller concentration of glycerin, is injected at a constant, and well controlled flow rate, by means of a glass syringe and a syringe pump. A three-way valve, which at the beginning of the experiment switches from injecting the more viscous fluid to its less viscous counterpart, is located very close to the inlet of the cell, in order to avoid any mixing of the fluids before they enter the cell. Experiments are conducted for the fluid combinations listed in Table I. Here, $c_g=x\%$ indicates a glycerin-water mixture with a mass concentration of glycerin of $x\%$. As dye we use amaranth, which in the present small concentrations does not affect the viscosity or density of the mixture. The Atwood number

$$\text{At}=\frac{\mu_1-\mu_2}{\mu_1+\mu_2} \tag{1}$$

represents the dimensionless viscosity difference between the two fluids. For some of the results to be discussed below, it will be advantageous to represent various quantities as a function of the viscosity ratio

$$M=\frac{\mu_1}{\mu_2} \tag{2}$$

instead of At, which is why Table I provides the values of both of these parameters for the experiments.

For each fluid combination, a number of experiments are conducted, at flow rates ranging from 0.26×10^{-3} to 392×10^{-3} cm^3/s. The Reynolds number, formed with the gap width and the viscosity of the less viscous fluid, varies between 10^{-2} and 10, so that for all but the largest flow rates inertial forces can be neglected. In this way, a wide range of Peclet numbers Pe is covered, where we define

$$\text{Pe}=Q/2\pi dD. \tag{3}$$

Here Q denotes the volumetric flow rate, and D represents the average coefficient of molecular diffusion. The factor of 2π is introduced to be consistent with the linear stability analysis by Tan and Homsy[31] for radially symmetric base flows, as well as with the numerical simulations of quarter five-spot displacements by Chen and Meiburg[10,11] and Pankiewitz and Meiburg.[32] The experiments are recorded on video tape for further analysis. For each experimental run, the time t_{end} is determined, at which the injected fluid first reaches the exit of the quarter five-spot configuration. Data will be presented both for the volumetric efficiency $\eta_{\text{vol}}=V_2/V_{\text{tot}}$, as well as the surface efficiency $\eta_{\text{sur}}=S_2/S_{\text{tot}}$ at breakthrough. Here V_2 indicates the injected volume of the less viscous fluid at t_{end}, while V_{tot} represents the total volume of the cell ($V_{\text{tot}}=6.1$ cm^3). S_2 denotes the normal projection of the region occupied by the less viscous fluid at time t_{end}, while S_{tot} is the surface area of the cell (100 cm^2). The mean ratio of the thickness of the injected fluid layer b to the gap width d can be calculated as $b/d=\eta_{\text{vol}}/\eta_{\text{sur}}$.

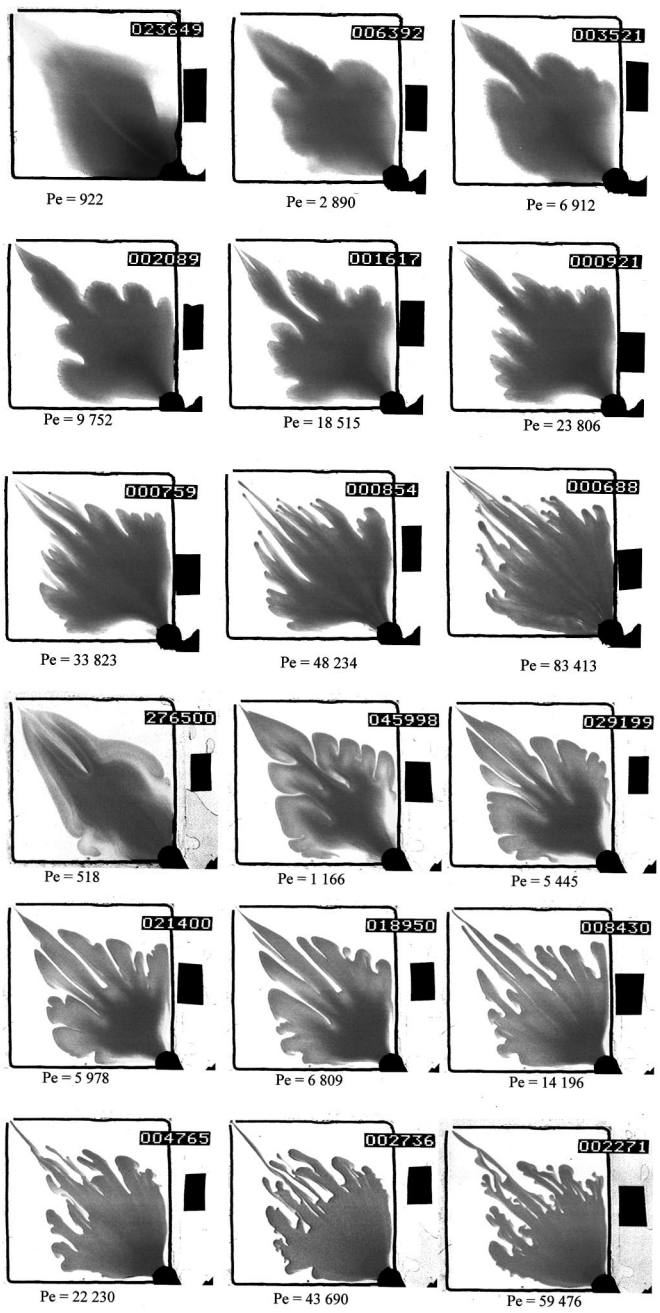

FIG. 3. (a) Fingering patterns at the breakthrough time t_{end} for different Peclet numbers. A water-dye mixture displaces a glycerin-water mixture of concentration $c_g = 66.4\%$. At$=0.848$. (b) Fingering patterns at the breakthrough time t_{end} for different Peclet numbers. A glycerin-water-dye mixture of concentration $c_g = 76.9\%$ displaces a glycerin-water mixture of concentration $c_g = 96\%$. At has the same value as in (a).

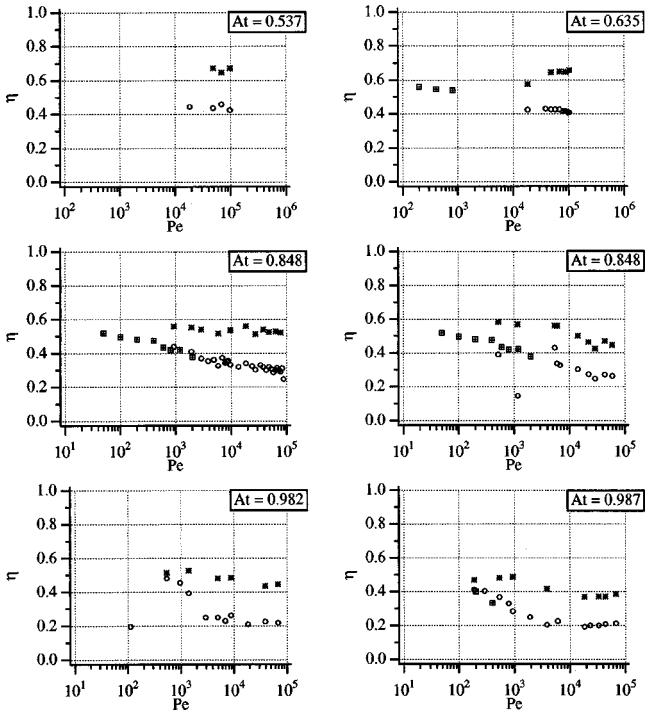

FIG. 4. Surface efficiency η_{sur} (*) and volume efficiency η_{vol} (○) as a function of the Pe for five different At values. The square symbols were obtained from the simulations of Chen and Meiburg (Ref. 10). Graphs (c) and (d) correspond to the same At, but the different fluid combinations of Figs. 3(a) and 3(b), respectively.

B. Results

As a representative example, Fig. 2 shows the temporal evolution of the flow for $At = 0.848$ and Pe$=13\,500$. We observe the development of a viscous fingering instability already during the early stages of the displacement. The growing fingers remain in competition for a certain time period, until a dominant structure evolves along the main diagonal, which eventually leads to the breakthrough of the less viscous fluid. The influence of Pe on the emerging flow pattern is demonstrated in Figs. 3(a) and 3(b). The differences between these two figures, which both have At$=0.848$, will be discussed below. A trend towards the growth of more and narrower fingers for increasing Pe is clearly visible in these figures, in agreement with the numerical simulations of Chen and Meiburg,[10] which did not account for the effects of flow-induced dispersion. For relatively low Pe values [$<10\,000$ in the experiments shown in Fig. 3(a)], only a few, wide fingers develop. For very large Pe($>40\,000$), on the other hand, the experiments depicted in Fig. 3(a), as well as additional ones not shown, suggest that the flow becomes largely independent of Pe, with both the number of fingers and their shape remaining nearly constant. An interesting observation concerns the dark, drop-shaped form of the tips of the fastest fingers at these large Pe, which indicates that the gap-averaged concentration of the less viscous fluid is higher there than in those finger sections behind the tip. There appear to be two potential explanations for this phenomenon: Either the finger tip could be thicker than the rest of the finger, i.e., the finger could have developed a bulge at the tip, perhaps due to an effective surface tension, cf. also the discussion below, or it could contain higher concentrations of the less viscous fluid. For some vertical flow configurations, and in the presence of density differences, the simulations of Chen and Meiburg,[21] as well as the experiments by Petitjeans and Maxworthy[20] for displacements in a capillary tube or a two-dimensional gap, display more intense mixing behind the finger tip than at the tip itself. However, it is not clear if a similar mechanism can occur for horizontal flows, or for negligible density differences.

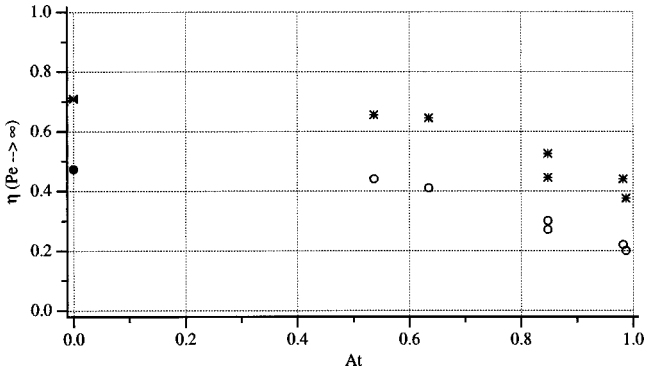

FIG. 5. Asymptotic surface (*) and volume (○) efficiencies as a function of At, for very large Pe. The value for At=0 was obtained on the basis of the potential flow results by Morel-Seytoux (Refs. 33 and 34).

More quantitative information is presented in Fig. 4, which depicts the volumetric and surface efficiencies as functions of Pe for five different At values. For the two smallest viscosity contrasts, the flow rates could not be reduced to values low enough to result in small Pe numbers. However, in the experiments for larger At, two distinct parameter ranges can be identified: For small Pe, the efficiencies decrease with increasing Pe, while for large Pe they asymptotically approach a constant value that depends on At only. The results of the two-dimensional simulations by

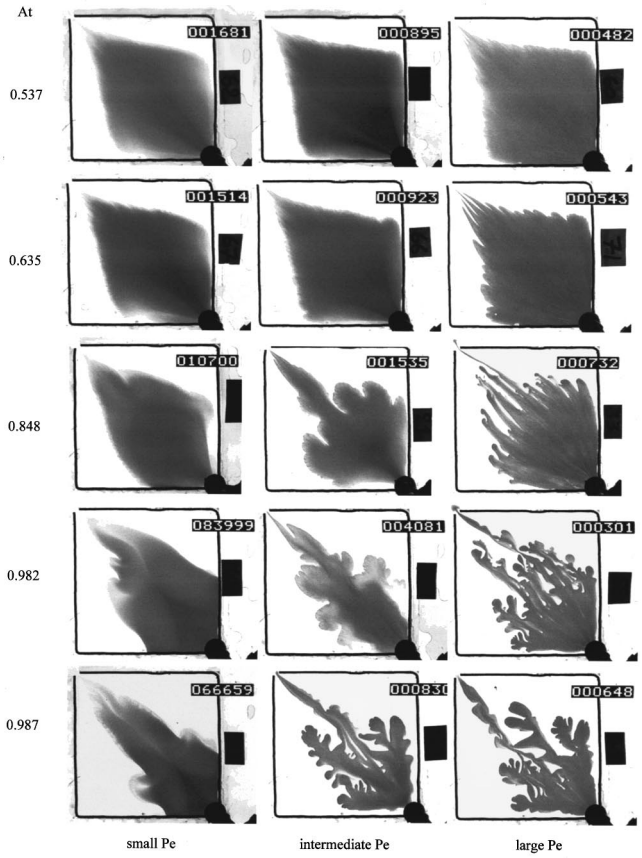

FIG. 6. Fingering patterns at breakthrough for the five different Atwood numbers of Fig. 4, and small, intermediate, and large Pe values, respectively. The less viscous fluid in all cases is a water-dye mixture.

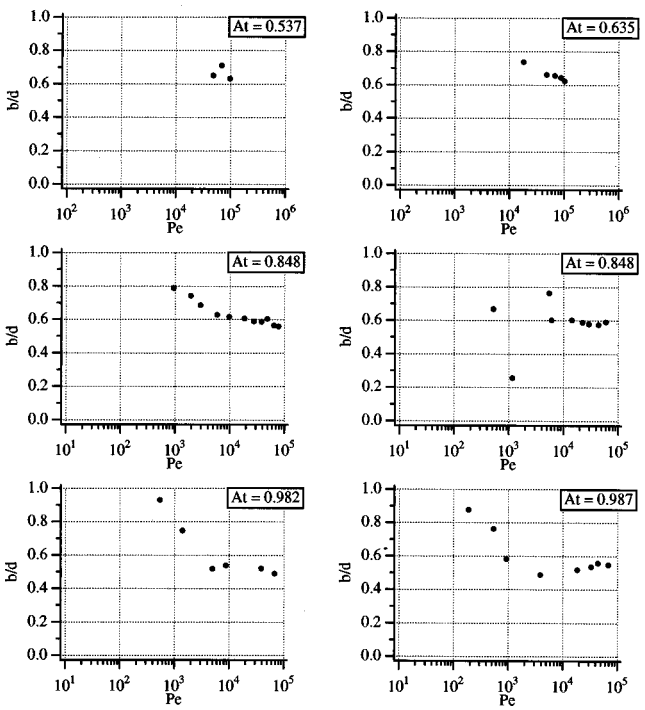

FIG. 7. Ratio of the average thickness b of the less viscous fluid layer to the gap width d, as a function of Pe, and for the six fluid combinations of Fig. 4.

Chen and Meiburg,[10] for which $\eta_{vol}=\eta_{sur}$, are plotted as well, and perhaps surprisingly, they agree better with the experimental data for the volumetric efficiency than for the surface efficiency.

Figure 5 shows the asymptotic efficiencies for very large Pe vs At. The values for At=0 are based on the analytical potential flow results of Morel-Seytoux[33,34] for the surface efficiency, along with the relationship $\eta_{vol}=\frac{2}{3}\eta_{sur}$ for Poiseuille flow in the gap. These asymptotic efficiencies decrease uniformly with At, with the ratio η_{vol}/η_{sur} declining as well.

Figure 6 depicts the flow at t_{end} for small, intermediate, and large Pe and five different At values, respectively. The general trend is towards a more unstable flow evolution as At increases. However, it is interesting to note that the radius of curvature at the finger tips tends to *increase* with At, i.e., with increasing concentration differences between the two fluids. In fact, for the largest At values the fingering patterns resemble those more typically observed in *im*miscible flows.[35,36] This behavior perhaps points towards the presence of additional stresses due to the large local concentration, viscosity, and density gradients, which may introduce an effective surface tension between the miscible fluids.[24–28,30] Regarding this issue, cf. also the discussion by Chen and Meiburg,[21] the determination of an effective surface tension coefficient by Petitjeans and Maxworthy,[20] and the direct measurement of such a coefficient by Petitjeans.[29]

The ratio of the average thickness of the less viscous fluid to the gap width, obtained from $b/d=\eta_{vol}/\eta_{sur}$, is plotted in Fig. 7. As expected, this ratio approaches an asymptotic value for large Pe, which is shown in Fig. 8 as a function of At. The result of $\frac{2}{3}$ for At=0 is obtained theoreti-

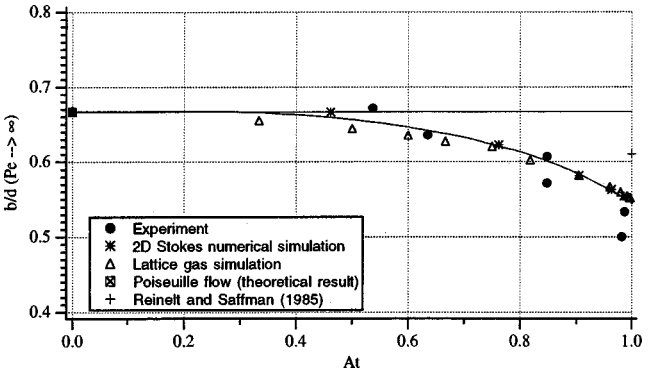

FIG. 8. Asymptotic thickness ratio b/d as a function of At for large Pe. Also plotted are the two-dimensional Stokes simulation results of Chen and Meiburg (Ref. 21), as well as the data obtained by Rakotomalala *et al.* (Ref. 23) via lattice gas simulations. The value for At=0 is obtained by assuming Poiseuille flow. Also shown is the computational result of Reinelt and Saffman (Ref. 27) for immiscible flow at large capillary number and At=1. Note: The theoretical and numerical results for rectilinear displacements.

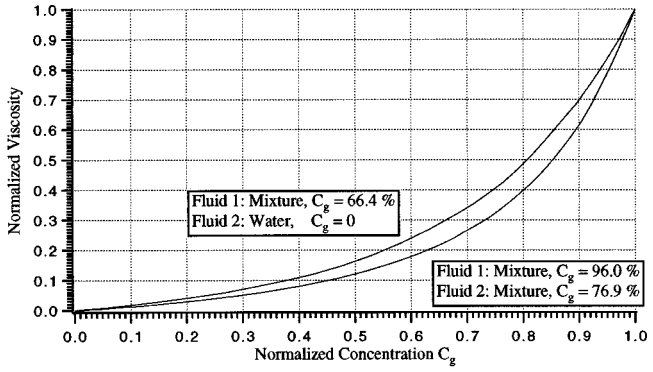

FIG. 9. Normalized viscosity as a function of the normalized concentration for the two different fluid combinations of Figs. 3(a) and 3(b), which gave rise to identical At values.

cally by assuming Poiseuille flow in the gap. For At$<$0.5, this ratio appears to remain nearly constant at a value of $\frac{2}{3}$, while it declines to almost 0.5 as At$\rightarrow$1. The Stokes simulation results of Chen and Meiburg,[21] plotted in the same graph, show good agreement with the experimental data, as do the values obtained from lattice gas calculations by Rakotomalala *et al.*[23] This suggests that up to values of At $\approx$0.5, the character of the flow in the gap is approximated well by a parabolic velocity profile, so that the assumption of Taylor dispersion should be valid in this parameter regime. This agrees with the results of Chen and Meiburg,[21] who find that for such relatively small viscosity contrasts a quasi-steady finger does not develop, and that the velocity profiles remain nearly parabolic. A near-parabolic nature of the velocity profile across the gap for Atwood numbers up to approximately 0.5 is also suggested by the η_{sur} value for At $=0.537$, which is still near the value of 0.718 that holds if the gap-averaged velocity field is irrotational.[33,34] The result obtained by Reinelt and Saffman[37] for immiscible flow at At=1 and large capillary number is plotted as well. Interestingly, the results for immiscible flow at high capillary number and for miscible flow at high Pe do not seem to converge towards the same value as At$\rightarrow$1. This is different from the axisymmetric case, for which we found good agreement of these two limits.[21] The determination of an effective surface tension for the miscible flow by Petitjeans and Maxworthy[20] had been based on this agreement.

We now return to the differences between the results shown in Figs. 3 and 4 for identical At values, but different fluid combinations. In Fig. 3(a) water ($\mu_2=1$ cP) displaces a glycerin-water mixture of $\mu_1=12.2$ cP, while in Fig. 3(b) a glycerin-water mixture of $\mu_2=29.4$ cP displaces a more concentrated glycerin-water mixture of $\mu_1=357.5$ cP. The difference in the asymptotic surface and volume efficiency values obtained for these two fluid pairs is too large to be explained by random variations between individual experimental runs. It hence demonstrates that Pe and At are not sufficient to fully describe the experimental observations, and that other, potentially important effects need to be considered. One possible reason for the observed discrepancy may lie in the different density contrasts of the two fluid pairs, which could trigger gravitational effects. In Fig. 3(a), the densities are 1.17 g/cm^3 for the more viscous, and 1 g/cm^3 for the less viscous fluid. In Fig. 3(b), on the other hand, the respective densities are 1.25 and 1.2 g/cm^3. In the horizontal Hele-Shaw cell arrangement, one of the interfaces forming between the two fluids hence is subject to a gravitational instability. In our case, the more viscous fluid always is also the heavier one, so that the upper interface is gravitationally unstable. The evolving instability leads to the formation of streaks in the direction of the flow. This effect has also been observed by Kurowski and Obernaer,[38] who found the wavelength of the instability to be on the order of the gap width of the Hele-Shaw cell. In the context of sedimenting flows, corresponding results are reported by Chandler.[39] This gravitational instability promotes more intense mixing between the two fluids along the upper side of the finger. As is evident from Fig. 7, however, the effective thickness of the less viscous fluid remains unaffected by this enhanced mixing. Consequently, the results for the surface and volume efficiencies suggest that the enhanced mixing effectively leads to a smaller viscosity contrast, which in turn results in improved efficiency values at breakthrough.

Another possible reason lies in the different shapes of the viscosity profiles as a function of concentration, shown in Fig. 9. Here the concentrations are normalized in such a way that the displacing fluid corresponds to $c=0$ and the resident fluid to $c=1$, respectively. The viscosities are normalized by that of the displacing fluid. However, this effect should not be significant at large Pe, when the concentration boundary layers are quite thin. This is confirmed by Stokes flow simulations we conducted for miscible flows in a two-dimensional gap, corresponding to the earlier results reported by Chen and Meiburg.[21] Even for moderate Peclet numbers of $O(2000)$ and At=0.905, these simulations gave the similar values for b/d of 0.58 for an exponential viscosity-concentration relationship, and 0.60 for a linear relationship. A further possibility concerns differences in the molecular diffusion coefficients. In the case of water displacing a glycerin-water mixture of $c_g=66.4\%$, the average coefficient of molecular diffusion is approximately 10^{-5} cm^2/s. For the

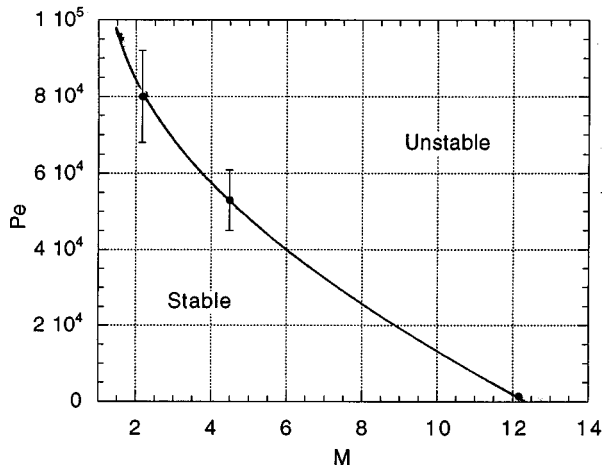

FIG. 10. The critical Pe value, beyond which a fingering instability is observed, as a function of the viscosity ratio.

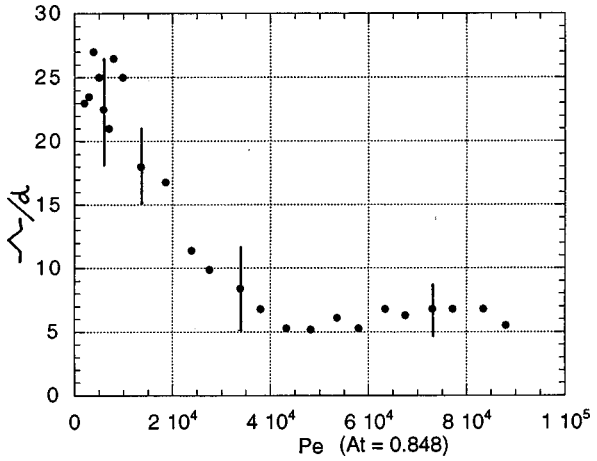

FIG. 12. The dominant finger width at the time of breakthrough, as a function of Pe, for At=0.848.

case in which a glycerine-water mixture of $c_g=76.9\%$ displaces a more viscous glycerin-water mixture of $c_g=96\%$, $D=1.2\times10^{-6}$ cm^2/s.[20] However, this effect should not be significant either at large Pe values. Finally, the possibility needs to be mentioned that the observed discrepancies between the two cases of At=0.848 may be related to the additional stresses at the miscible interface referred to above, i.e., an effective surface tension between the two fluids.

As mentioned in the Introduction, there are several investigations in the literature with which we can compare our measurements. The experiments by Zhang *et al.*[9] were carried out in a relatively thick, saturated, homogeneous quarter five-spot Hele-Shaw cell packed with beads. The flow visualization pictures presented in their paper are quite similar to ours, for a similar At range, although the tips of the fingers are much more circular in our experiments. This is probably due to the absence of beads in our Hele-Shaw cell. The volumetric efficiency as a function of At is in good agreement with our measurements for large Atwood numbers, and in the asymptotic Pe regime. For smaller At values, the agreement is less satisfactory, as Zhang *et al.* record efficiencies significantly larger than ours. Possibly their experiments do not yet fall into the asymptotic Pe regime. Habermann's[5] experiments were conducted in a quarter five-spot configuration for an artificially consolidated sand model. For large At values, their recorded volumetric efficiencies agree well with ours, while for smaller Atwood numbers again there are significant differences. Regarding the surface efficiency, there are differences across the entire spectrum of At numbers. Mahaffey's *et al.*[7] experiments were carried out in Hele-Shaw cells of two different gap widths. The authors' data for the volumetric efficiency at breakthrough as a function of At are in good agreement with our asymptotic values.

A final interesting point concerns the preferred wavelength λ selected by the fingering instability in Hele-Shaw displacements. This question has been addressed extensively in the past, e.g., by Park and Homsy,[40] Paterson,[41] and Schwartz.[42] A review of these earlier pertinent experimental and theoretical results is provided by Maxworthy.[43] Additional light has been shed on this issue by the more recent

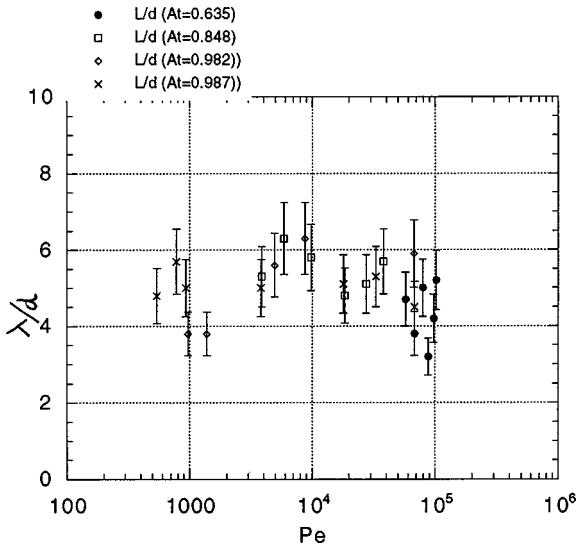

FIG. 11. The preferred wavelength of the observed fingering instability varies between approximately four and six times the gap width, and is largely independent of Pe and At.

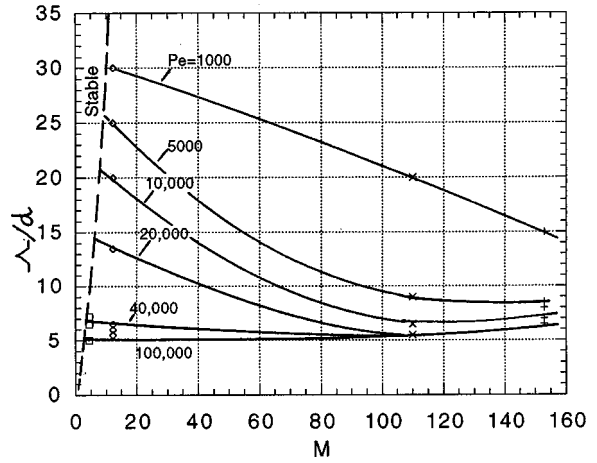

FIG. 13. The dominant finger width at the time of breakthrough, as a function of both Pe and the viscosity ratio.

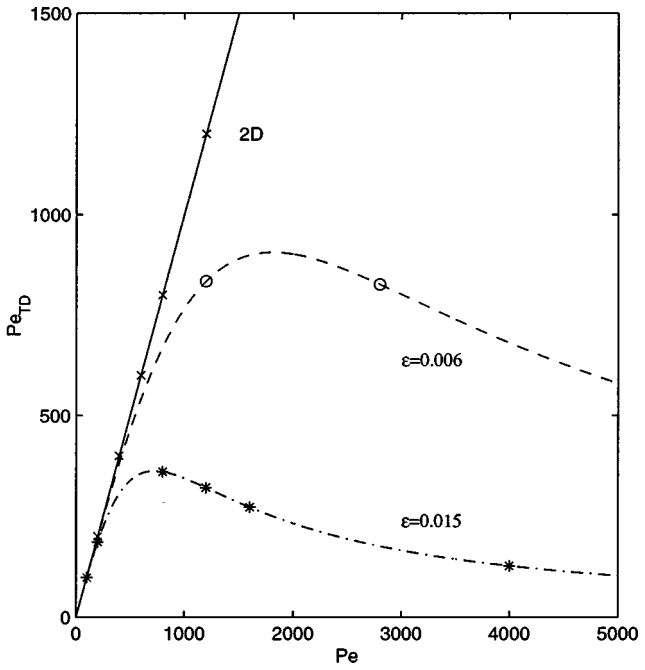

FIG. 14. Pe_{TD} as a function of Pe, for the two different aspect ratio values of $\epsilon = 0.006$ and 0.015. The characteristic velocity is assumed to have a value of 2.

work of Lajeunesse *et al.*[44,45] on vertical miscible displacements in Hele-Shaw cells. These authors observe that above a viscosity ratio of approximately 1.5 there exists a critical displacement velocity, beyond which the interface develops a three-dimensional instability with a preferred wavelength of about five times the cell thickness. Snyder and Tait[46] study gravity currents of a less viscous fluid into a more viscous one in a Hele-Shaw cell, and they observe a preferred wavelength of the frontal instability of approximately twice the current height.

In analogy with the rectilinear displacements studied by Lajeunesse *et al.*,[44,45] the present experiments in the quarter five-spot geometry demonstrate the existence of a viscosity ratio dependent critical dimensionless flow rate, beyond which the displacement process develops a three-dimensional instability, cf. Fig. 10. The data furthermore suggest that above a viscosity ratio of approximately 12, the displacement is unstable at all values of Pe. In agreement with earlier observations, both by us as well as by other authors, the dominant wavelength λ of the observed instability is found to be between four and six times the gap width d, independent of the viscosity ratio and the dimensionless flow rate, cf. Fig. 11. Interestingly, however, this preferred wavelength observed at small amplitudes of the instability does not necessarily determine the dominant width Λ of the fully developed fingers seen at later times. Figure 12 presents data for Λ at the time of breakthrough, obtained from the experimental video frames, as a function of Pe, for the viscosity ratio of 12.2. It shows that for small Pe, the finger width decreases uniformly with increasing flow rate, and it reaches its asymptotic value of about six times the gap width only above $Pe \approx 4 \times 10^4$. Figure 13, which is obtained by cross-plotting figures such as Fig. 12 for different viscosity ratios, summarizes the data for the dominant finger width as a function of both Pe and the viscosity ratio.

III. NUMERICAL SIMULATIONS

In this section, we report on numerical simulations of quarter five-spot displacements that account for flow-induced dispersion by applying the approach taken by Zimmerman and Homsy[19] in their simulations. Some interesting features of the underlying dispersion model will be pointed out, and a comparison of the numerical results with the above experimental measurements will provide information regarding the parameter range over which it is applicable to miscible, variable viscosity Hele-Shaw displacements involving fluids of different viscosities.

A. Taylor dispersion model

Zimmerman and Homsy[19] propose to account for flow-induced dispersion by formulating the concentration equation in terms of a velocity-dependent dispersion tensor **D**, whose components are evaluated on the basis of the classical Taylor dispersion results obtained by Horne and Rodriguez[13] for Poiseuille flow in a two-dimensional gap. The concentration equation thus takes the form

$$\frac{\partial c}{\partial t} + \vec{u} \cdot \nabla c = \nabla \cdot (\mathbf{D} \nabla c), \tag{4}$$

where **D** is of the form

$$\mathbf{D} = \mathbf{R}^* \mathbf{D}_p \mathbf{R}, \tag{5}$$

$$\mathbf{R} = \frac{1}{|\mathbf{u}|} \begin{bmatrix} u & v \\ -v & u \end{bmatrix}, \tag{6}$$

$$\mathbf{D}_p = \begin{bmatrix} D_\parallel & 0 \\ 0 & D_\perp \end{bmatrix}, \tag{7}$$

$$D_\parallel = D + \frac{2}{945} \frac{d^2 U^2}{D}, \quad D_\perp = D. \tag{8}$$

Here U is the velocity at the center of the gap, and D represents the molecular diffusion coefficient. u and v denote the Cartesian velocity components. In the flow direction, the evolution of the concentration profile is determined by the longitudinal dispersion coefficient $D_\parallel$, which represents the superimposed effects of molecular diffusion as well as Taylor dispersion. In the direction normal to the flow, the transverse diffusion coefficient $D_\perp$ accounts for only molecular diffusion. Questions regarding the range of applicability of this approach arise because Taylor's,[12] as well as Horne and Rodriguez's,[13] work assumes constant viscosities, so that the flow is of Poiseuille type everywhere. In the presence of strong viscosity contrasts and at high Pe values, on the other hand, the work by Petitjeans and Maxworthy,[20] Chen and Meiburg,[21] Yang and Yortsos,[22] as well as Rakotomalala *et al.*[23] indicates that the velocity profiles can be quite different from Poiseuille flow.

The above model for flow-induced dispersion gives an effective Taylor dispersion Peclet number Pe_{TD}

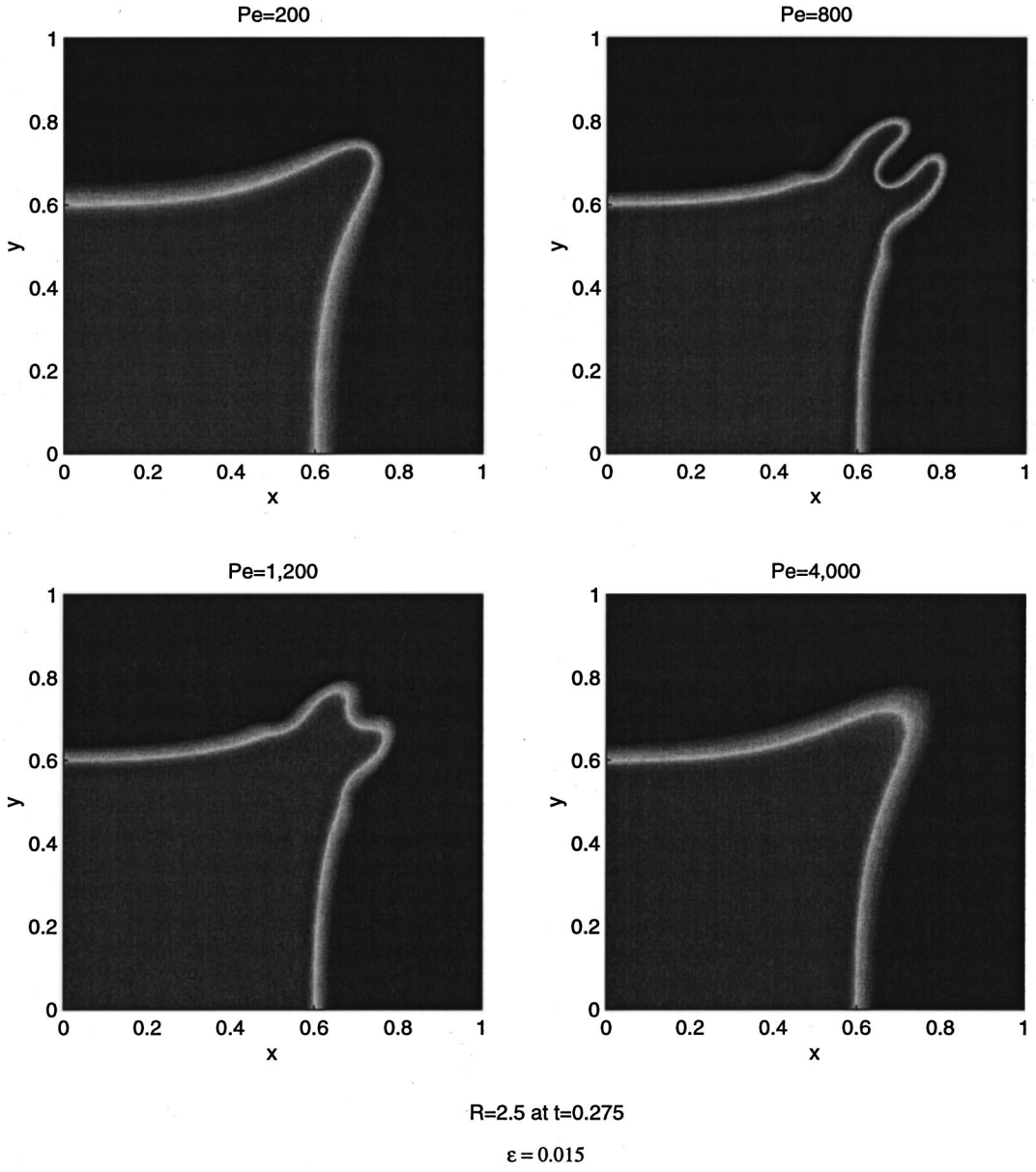

FIG. 15. At=0.848, $\epsilon=0.015$, and $t=0.275$ for all frames. (a) Fingering configuration for Pe=200 ($Pe_{TD}=186$). (b) Pe=800 ($Pe_{TD}=361$). (c) Pe=1200 ($Pe_{TD}=320$). (d) Pe=4000 ($Pe_{TD}=127$).

$$Pe_{TD} \equiv \frac{Q}{2\pi d D_{\parallel}} = \frac{Pe}{1+\frac{2}{945}Pe^2\epsilon^2(u^2+v^2)}, \tag{9}$$

where ϵ denotes the ratio of the gap width and the side length of the quarter five-spot arrangement. Since it depends on the dimensionless velocity magnitude, Pe_{TD} varies throughout the flowfield. However, along large sections of the diagonal, where Taylor dispersion effects are strongest, the dimensionless fluid velocity in all simulations is on the order of two, without much variation for different At or Pe values. This weak dependence of the dimensionless velocity on Pe and At is confirmed by Fig. 4, which shows that the efficiencies do not change by more than a factor of approximately two for different At values, and Peclet numbers spanning several orders of magnitude. Consequently, we can take this value of 2 as a characteristic one for the dimensionless velocity, in order to relate Pe to a globally relevant value of Pe_{TD}. Hence, for sufficiently low Pe we have $Pe_{TD} \approx Pe$, while large Peclet numbers result in $Pe_{TD} \propto 1/Pe$. Thus there exists a value Pe=Pe*,

$$Pe^* = \sqrt{\frac{945}{2\epsilon^2(u^2+v^2)}}, \tag{10}$$

for which Pe_{TD} attains a maximum value

$$Pe_{TDmax} = \frac{Pe^*}{2}. \tag{11}$$

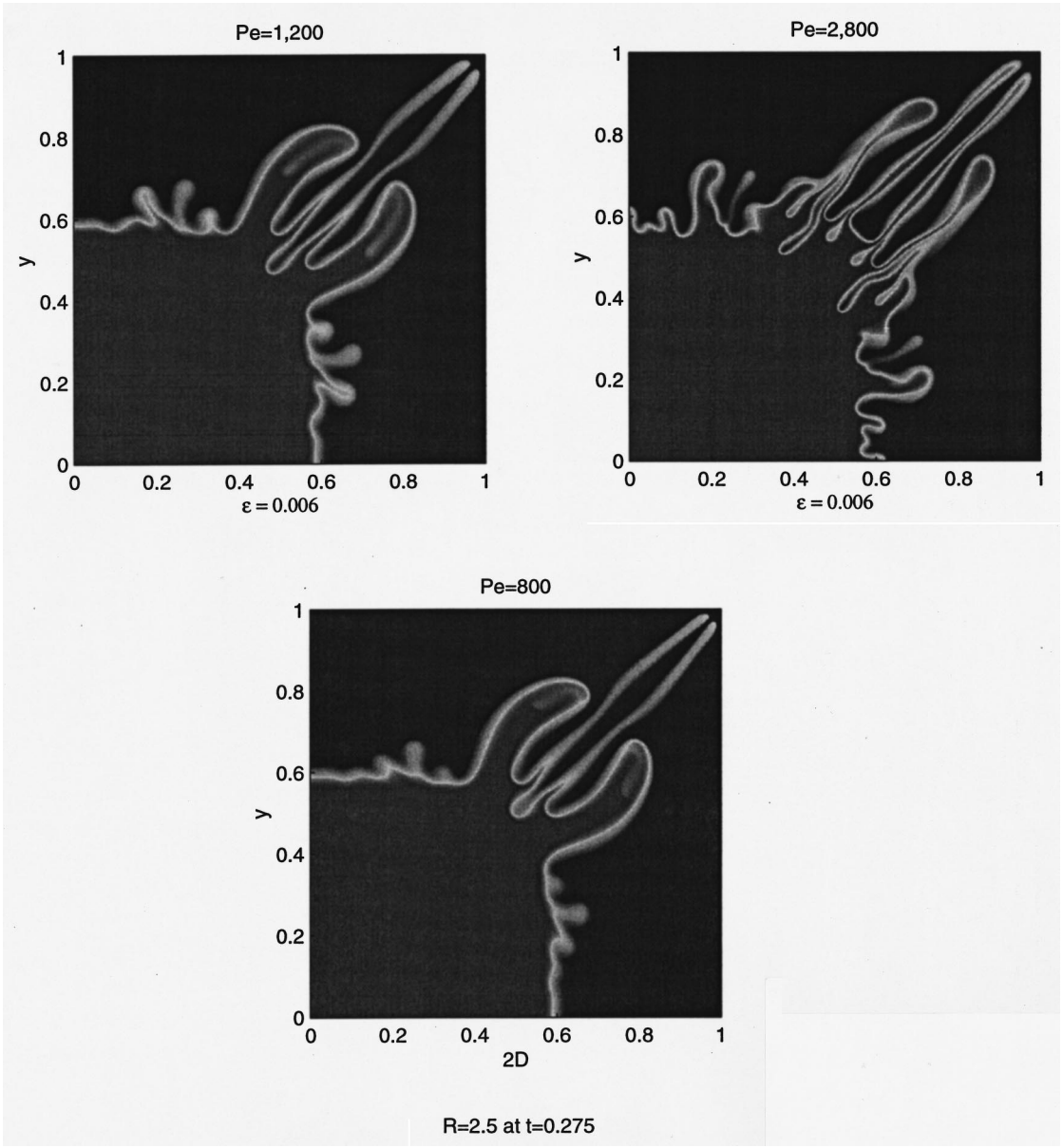

FIG. 16. Fingering configuration for (a) At=0.848, $\epsilon=0.006$, Pe=1200 ($Pe_{TD}=834$). (b) At=0.848, $\epsilon=0.006$, Pe=2800 ($Pe_{TD}=826$). (c) At=0.848, Pe=800, no Taylor dispersion (from Ref. 10).

In the following, we will discuss properties of the Taylor dispersion model by presenting numerical results for several values of Pe_{TD}, corresponding to different combinations of Pe and ϵ, and comparing them with the experimental observations described above. For details regarding the numerical method, which is based on a combination of spectral methods[47] and compact finite differences,[48] we refer to Ref. 49. As in our earlier simulations, an exponential relationship between concentration and viscosity will be assumed, and the starting time for the simulations is held fixed at a dimensionless value of 0.02, when a radially symmetric concentration profile is prescribed. For further details, cf. Refs. 10 and 11. At=0.848, which corresponds to a value of $R=2.5$ in those earlier simulations.

B. Results

As a first step, we consider displacements for an aspect ratio ϵ of 0.015. For Pe=200, Fig. 14 indicates that this value of ϵ results in $Pe \approx Pe_{TD}=186$. Consequently, a stable front evolves [Fig. 15(a)] that is very similar to the one observed for Pe=200 in the absence of Taylor dispersion.[10] If Pe is increased to 800 and 1200, respectively, a single front splitting event takes place. Interestingly, this splitting occurs at a somewhat *later* time for Pe=1200 than for Pe=800, cf. Figs. 15(b) and 15(c). This indicates that the displacement is *more stable* for the larger Pe value. Figure 14 provides the explanation for this observation, as it shows that Pe_{TD} reaches a maximum of about 362 for $Pe \approx 725$. It subsequently decreases for increasing Pe values, so that for Pe =800 and 1200, we have $Pe_{TD}=361$ and 320, respectively. For Pe=4000, we get $Pe_{TD}=127$, which again results in a stable front, with a concentration profile that is fairly thick near the diagonal, cf. Fig. 15(d). While the frontal shapes for $Pe=200$ and 4000 are quite similar, there is a fundamental difference between these two stable cases. For the lower Pe-

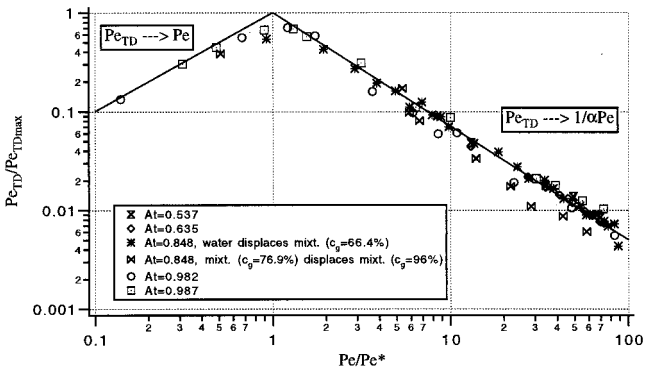

FIG. 17. Pe_{TD}/Pe_{TDmax} as a function of Pe/Pe*, for all experiments. The solid lines indicate the respective asymptotic behaviors at very large and at small Pe/Pe*. For the larger At values, the experimental parameters cover both of those regimes.

clet number, molecular diffusion dominates over flow-induced dispersion. An analysis of the velocity field in the neighborhood of the front near the main diagonal shows that the front is compressed by the local strain field in this region, resulting in a fairly steep concentration profile. Along the sides of the quarter five-spot geometry, there is no such strain compression, so that the front is considerably thicker there. For Pe=4000, on the other hand, Taylor dispersion dominates over molecular diffusion. Consequently, the larger flow velocities along the main diagonal cause a locally thicker front here, whereas steeper concentration profiles are found near the edges, where the fluid velocity and related dispersion are small.

We now consider the smaller aspect ratio $\epsilon=0.006$, which closely corresponds to the experimental value of 0.0061. Figures 16(a) and 16(b) depict concentration fields for Pe=1200 ($Pe_{TD}=834$) and Pe=2800 ($Pe_{TD}=826$), respectively. These comparable Pe_{TD} values result in very similar fingering patterns near the main diagonal, which also bear a strong resemblance to the Pe=800 results reported by Chen and Meiburg[10] in the absence of flow-induced dispersion, cf. Fig. 16(c). Far away from the diagonal, however, where the flow velocities and the related Taylor dispersion are small, the highest Pe simulation shows somewhat more intense fingering. The breakthrough times of all three of the above cases are almost identical.

Focusing on the effect of ϵ, we notice that for a fixed flow rate, i.e., Pe=const, smaller values of ϵ result in larger Taylor dispersion Peclet numbers Pe_{TD}, thereby encouraging more vigorous fingering. This is clearly demonstrated by the simulations for Pe=1200 and $\epsilon=0.015$ and 0.006, respectively.

IV. DISCUSSION AND CONCLUSIONS

Interestingly, the above numerical simulations for At =0.848 at relatively large Pe values, which are based on the Taylor dispersion assumption, show that the flow becomes *more* stable with increasing Pe at this large viscosity contrast. In order to assess the range of applicability of the Taylor dispersion model, this finding will now be discussed in light of the experiments described above. Assuming the Taylor dispersion model is applicable, we can define a global Taylor dispersion Peclet number Pe_{TD} for the experiments on the basis of a characteristic dimensionless velocity $U=2^{1/2}dL^2/Qt_{end}$. Figure 17 shows the values of Pe/Pe* and Pe_{TD}/Pe_{TDmax} for the experimental runs. It confirms that, for the larger At values, the experiments cover both of the regimes described above: For relatively small Peclet numbers, they fall into the range where $Pe_{TD}\rightarrow Pe$, whereas the large Peclet number runs follow $Pe_{TD}\propto 1/Pe$. However, for these large At values the experiments do not show that the flow becomes more stable with increasing Pe, as the numerical results had suggested. This confirms what we suspected on the basis of Figure 8, namely that for Hele-Shaw flows at large Peclet numbers, Taylor dispersion represents a good approximation to the evolution of the gap-averaged concentration profile up to At≈0.5, but not beyond. In order to extend the range of validity of the dispersion tensor to larger At values, its components will have to be modified to account for the formation of the quasi-steady fingers reported by Petitjeans and Maxworthy[20] as well as Chen and Meiburg[21] under these conditions.

ACKNOWLEDGMENTS

This work was made possible by NASA, through Grant No. 53-4514-8880. The authors furthermore wish to acknowledge partial support from a NATO Collaborative Research Grant, the donors of The Petroleum Research Fund (Grant ACS-PRF No. 33497-AC9), and the Chevron Petroleum Technology Company. The simulations were carried out at the San Diego Supercomputer Center, which is supported by the National Science Foundation.

[1] G. M. Homsy, ''Viscous fingering in porous media,'' Annu. Rev. Fluid Mech. **19**, 271 (1987).
[2] Y. C. Yortsos, ''Instabilities in displacement processes in porous media,'' J. Phys.: Condens. Matter **2**, SA 443 (1990).
[3] B. H. Caudle and M. D. Witte, ''Production potential changes during sweep-out in a five-spot system,'' Trans. AIME **216**, 446 (1959).
[4] J. Simmons, B. L. Landrum, J. M. Pinson, and P. B. Crawford, ''Swept areas after breakthrough in vertically fractured five-spot patterns,'' Trans. AIME **216**, 73 (1959).
[5] B. Habermann, ''The efficiency of miscible displacement as a function of mobility ratio,'' Trans. AIME **219**, 264 (1960).
[6] J. W. Lacey, J. E. Faris, and F. H. Brinkman, ''Effect of bank size on oil recovery in the high-pressure gas-driven LPG-bank process,'' Trans. AIME **222**, 806 (1961).
[7] J. L. Mahaffey, W. M. Rutherford, and C. S. Matthews, ''Sweep efficiency by miscible displacement in a five-spot,'' Soc. Pet. Eng. J. (3), 73 (1966).
[8] M. R. Todd and W. J. Longstaff, ''The development, testing and application of a numerical simulator for predicting miscible flood performance,'' Soc. Pet. Eng. J. **12**, 874 (1972).
[9] H. R. Zhang, K. S. Sorbie, and N. B. Tsibuklis, ''Viscous fingering in five-spot experimental porous media: New experimental results and numerical simulation,'' Chem. Eng. Sci. **52**, 37 (1997).
[10] C.-Y. Chen and E. Meiburg, ''Miscible porous media displacements in the quarter five-spot configuration. Part 1: The homogeneous case,'' J. Fluid Mech. **371**, 233 (1998).
[11] C.-Y. Chen and E. Meiburg, ''Miscible porous media displacements in the quarter five-spot configuration. Part 2: Effects of heterogeneities,'' J. Fluid Mech. **371**, 269 (1998).
[12] G. I. Taylor, ''Dispersion of soluble matter in solvent flowing slowly through a tube,'' Proc. R. Soc. London, Ser. A **219**, 186 (1953).
[13] R. N. Horne and F. Rodriquez, ''Dispersion in tracer flow in fractured geothermal systems,'' Geophys. Res. Lett. **10**, 289 (1983).

[14]J. F. Brady and D. L. Koch, in *Disorder and Mixing*, edited by E. Guyon *et al.*, NATO ASI Series E (Academic, New York, 1988).
[15]D. W. Peaceman and H. H. Rachford, ''Numerical calculation of multidimensional miscible displacement,'' Soc. Pet. Eng. J. (12), 327 (1962).
[16]R. E. Ewing, T. F. Russell, and L. C. Young, ''An anisotropic coarse-grid dispersion model of heterogeneity and viscous fingering in five-spot miscible displacement that matches experiments and fine-grid simulations, SPE Paper 18441.
[17]Y. Yortsos and M. Zeybek, ''Dispersion driven instability in miscible displacement processes,'' Phys. Fluids **31**, 3511 (1988).
[18]J. Bear, *Dynamics of Fluids in Porous Media* (Elsevier, New York, 1972).
[19]W. B. Zimmerman and G. M. Homsy, ''Nonlinear viscous fingering in miscible displacement with anisotropic dispersion,'' Phys. Fluids A **3**, 1859 (1991).
[20]P. Petitjeans and T. Maxworthy, ''Miscible displacements in a capillary tube. Part 1. Experiments,'' J. Fluid Mech. **326**, 37 (1996).
[21]C.-Y. Chen and E. Meiburg, ''Miscible displacements in a capillary tube. Part 2. Numerical simulations,'' J. Fluid Mech. **326**, 57 (1996).
[22]Z. Yang and Y. C. Yortsos, ''Asymptotic solutions of miscible displacements in geometries of large aspect ratio,'' Phys. Fluids **9**, 286 (1997).
[23]N. Rakotomalala, D. Salin, and P. Watzky, ''Miscible displacement between two parallel plates: BGK Lattice gas simulations,'' J. Fluid Mech. **338**, 277 (1997).
[24]D. Korteweg, ''Sur la forme que prennent les équations du mouvement des fluides si l'on tient compte des forces capillaires causées par des variations de densité,'' Arch. Neerl. Sci. Ex. Nat., Series II **6**, 1 (1901).
[25]H. T. Davis, ''A theory of tension at a miscible displacement front,'' in *Numerical Simulation in Oil Recovery*, IMA Volumes in Mathematics and its Applications 11, edited by M. Wheeler (Springer, Berlin, 1988).
[26]D. D. Joseph, ''Fluid dynamics of two miscible liquids with diffusion and gradient stresses,'' Eur. J. Mech. B/Fluids **9**, 565 (1990).
[27]D. D. Joseph and H. Hu, ''Interfacial tension between miscible liquids,'' Army High Performance Computing Research Centre, University of Minnesota, preprint 91-58 (1991).
[28]D. D. Joseph and Y. Y. Renardy, ''Fundamentals of two-fluid dynamics. Part II. Lubricated transport, drops, and miscible liquids,'' Springer series on *Interdisciplinary Applied Mathematics* (Springer, New York, 1993).
[29]P. Petitjeans, ''Une tension de surface pour les fluides miscibles,'' C. R. Acad. Sci., Ser. IIb: Mec., Phys., Chim., Astron. **322**, 673 (1996).
[30]P. Petitjeans and P. Kurowski, ''Fluides non miscibles fluides miscibles: des simulitudes intéressantes,'' C. R. Acad. Sci., Ser. IIb: Mec., Phys., Chim., Astron. **325**, 587 (1997).
[31]C. T. Tan and G. M. Homsy, ''Stability of miscible displacements in porous media: Radial source flow,'' Phys. Fluids **30**, 1239 (1987).
[32]C. Pankiewitz and E. Meiburg, ''Miscible porous media displacements in the quarter five-spot configuration. Part 3: Nonmonotonic viscosity profiles,'' J. Fluid Mech. **388**, 171 (1999).
[33]H. J. Morel-Seytoux, ''Analytical-numerical method in waterflooding predictions,'' Soc. Petr. Eng. J. (9), 247 (1965).
[34]H. J. Morel-Seytoux, ''Unit mobility ratio displacement calculations for pattern floods in homogeneous medium,'' Soc. Petr. Eng. J. (9), 217 (1966).
[35]L. Paterson, ''Radial fingering in a Hele-Shaw cell,'' J. Fluid Mech. **113**, 513 (1981).
[36]L. W. Schwartz and A. J. DeGregoria, ''Two-phase flow in Hele-Shaw cells: Numerical studies of sweep efficiency in a five-spot pattern,'' J. Aust. Math. Soc. B, Appl. Math. **29**, 375 (1988).
[37]D. A. Reinelt and P. G. Saffman, ''The penetration of a finger into a viscous fluid in a channel and tube,'' SIAM (Soc. Ind. Appl. Math.) J. Sci. Stat. Comput. **6**, 542 (1985).
[38]P. Kurowski and S. Obernaer, private communication (1995).
[39]F. O. Chandler, ''Convective instability of fluid interfaces,'' Ph.D. thesis, University of Southern California, 1998.
[40]C.-W. Park and G. M. Homsy, ''Two-phase displacements in Hele-Shaw cells: Theory,'' J. Fluid Mech. **139**, 291 (1984).
[41]L. Paterson, ''Fingering with miscible fluids in a Hele-Shaw cell,'' Phys. Fluids **28**, 26 (1985).
[42]L. Schwartz, ''Stability of Hele-Shaw flows: The wetting-layer effect,'' Phys. Fluids **29**, 3086 (1986).
[43]T. Maxworthy, ''Experimental study of interface instability in a Hele-Shaw cell,'' Phys. Rev. A **39**, 5863 (1989).
[44]E. Lajeunesse, J. Martin, N. Rakotomalala, and D. Salin, ''3D instability of miscible displacements in a Hele-Shaw cell,'' Phys. Rev. Lett. **79**, 5254 (1997).
[45]E. Lajeunesse, J. Martin, N. Rakotomalala, D. Salin, and Y. C. Yortsos, ''Miscible displacement in a Hele-Shaw cell at high rates,'' preprint (1998).
[46]D. Snyder and S. Tait, ''A flow-front instability in viscous gravity currents,'' J. Fluid Mech. **369**, 1 (1998).
[47]D. Gottlieb and S. A. Orszag, *Numerical Analysis of Spectral Methods* (SIAM, Philadelphia, 1977).
[48]S. K. Lele, ''Compact finite difference schemes with spectral-like resolution,'' J. Comput. Phys. **103**, 16 (1992).
[49]E. Meiburg and C. Y. Chen, ''High-accuracy implicit finite difference simulations of homogeneous and heterogeneous miscible porous media flows,'' submitted to SPE Res. Eng.